

Near-field Anchor-free Localization using Reconfigurable Intelligent Surfaces

Srikar Sharma Sadhu, Praful D. Mankar, and Santosh Nannuru

Abstract—Near-field localization is expected to play a crucial role in enabling a plethora of applications under the paradigm of 6G networks. The conventional localization methods rely on complex infrastructure for providing cooperative anchor nodes that often contribute to higher network overload and energy consumption. To address this, the passive reconfigurable intelligent surfaces (RISs) can be leveraged as perfectly synced reference nodes for developing anchor-free localization. This work proposes a two-stage framework for localizing user equipment (UE) equipped with multiple antennas. At first, we show that the optimal RIS phase shift matrix maximizing the received signal-to-noise ratio (SNR) for RIS-assisted anchor-free localization is independent of UE location, making the proposed framework scalable without increasing the overhead to control RIS. The proposed two-stage framework first obtains a coarse estimate of UE’s location by correlating the received RIS-reflected signal with a dictionary constructed using line-of-sight (LoS) components at a few reference positions. Next, the coarse estimate is refined using Newton’s refinement. The numerical results show that the small-sized dictionary, constructed using fewer reference positions, can be employed for accurate localization with a slight increase in the required number of refinement iterations.

Index Terms—RIS, near-field localization, anchor-free localization.

I. INTRODUCTION

Radio localization is emerging as an alternative to GPS-based localization, especially in environments like indoor scenario where wireless networks can be accessed more reliably as compared to satellite signals [1]. Localization is expected to play an important role in the integration of cellular communication with a plethora of new applications emerging under 6G paradigm such as sensing, object mapping, massive IoT, etc., [2], [3]. However, the conventional localization approaches rely on multiple active anchors such as base stations (BSs) and access points (APs) that often have high hardware complexity and energy consumption, and requires tight synchronization [4]–[6]. Interestingly, the advent of reconfigurable intelligent surfaces (RISs) offers an attractive solution to this problem where the passive RISs can be utilized as the tightly synced reference points for localization. In particular, the signals reflected off the passive RIS surfaces can be utilized for triangulation and estimating the angle of arrival (AoA), angle of departure (AoD), time difference of arrival etc. without explicitly requiring synchronization. Motivated by this, we focus on utilizing RIS for realizing *anchor-free localization*.

S. S. Sadhu, P. D. Mankar and S. Nannuru are with Signal Processing and Communication Research Center, IIT Hyderabad, India. Email: srikar.sadhu@research.iiit.ac.in, {praful.mankar,santosh.nannuru}@iiit.ac.in.

A. Related Works

Conventional radio localization wherein an agent tries to localize itself using a set of active anchors has been explored thoroughly in literature for a variety of system settings. Interested readers may refer to [6]–[8] for a comprehensive survey along these lines. Additionally, the authors of [9]–[12] present anchor-free localization which involves the user equipment (UE) localizing itself in the absence of BSs or APs. The authors of [9], [10] use a cooperative environment for localizing the UEs via assistance of a special node that is either GPS-enabled or acts as a central hub. Alternatively, the authors of [11], [12] rely on the ultra-wideband protocol in anchor-free environments. In particular, [11] presents trilateration based simultaneous localization and mapping (SLAM), whereas [12] utilizes peer-to-peer range measurements to perform 3D pose estimation. However, these works still require a certain level of cooperation. This either requires the infrastructural dependencies for tagging at least one node or peer-to-peer communication, which essentially limits these works from truly being anchor-free localization.

In contrast, the RIS can facilitate localization without requiring the system level dependence [13] where the UE can use the signal reflected from RIS to localize itself with respect to RIS position — even the UE location based dynamic RIS control is not necessary (as will be shown in this paper). However, this line of research remains to be explored in the literature to its fullest potential. For example, [14]–[17] are the only available works on RIS-assisted anchor-free localization. The authors of [14]–[16] developed frameworks wherein they utilize the prior knowledge of the UE location to optimally configure the RIS and then employ two-stage approach involving coarse estimation and its refinement via iterative algorithms under optimally configured RIS. In particular, the authors of [14] obtain the coarse estimate using delay profile that is obtained via the inverse fast Fourier transform of the received signal. Next, the authors refine the coarse estimate by maximizing the likelihood function. In [15], the authors develop anchor-free SLAM wherein the RIS phase shifts require to be dynamically configured based on the UE state. The UE state and landmarks are estimated using a modified marginal Poisson multi-Bernoulli SLAM filter. While [14], [15] use full duplex UE for RIS-assisted localization/SLAM, the authors of [16] consider half-duplex UE localization with cooperation from multiple other UEs for receiving the signal reflected from RIS to facilitate the maximum likelihood estimation of the UE’s location. On the

other hand, the authors of [17] consider the reception of signal reflected from RIS at full-duplex UE under a phase shift codebook that sweeps the entire angular region. This facilitates the UE to construct a delay-Doppler map corresponding to the non-stationary objects in the environment, which is further used to localize the UE. Although, these works present novel approaches, the RIS phase shift needs to be dynamically controlled depending on the UE location [14]–[16]. This requires frequent adaptation and leads to increased overhead and computational complexity.

Motivated by this, we present a robust approach for RIS-assisted anchor-free near-field localization wherein the signal reflected from the pre-configured RIS's surface is utilized for localization without the need for frequent RIS control, as opposed to the previous works. In particular, we developed a simple yet effective approach that first obtains a coarse estimate of UE location by correlating the received signal from the pre-configured RIS with the dictionary constructed using line-of-sight (LoS) channels in near-field region of RIS. Next, we employ Newton refinement to iteratively refine the coarse estimate. Through extensive numerical analysis, we show that the proposed approach provides low normalized mean square error (NMSE) performance that is not affected by enlarging the near-field region (i.e. by increasing RIS size), which ensures that the proposed solution is scalable to practical settings. Further, the numerical results demonstrate that a small-sized dictionary, constructed using a fewer reference positions, can be employed without significant degradations in NMSE performance, albeit with a slight increase in the required number of refinement iterations.

B. Notation

Vectors are denoted using bold lowercase letters (e.g. \mathbf{q}) and matrices are denoted using bold uppercase letters (e.g. \mathbf{Q}). Transpose, conjugate, conjugate transpose and pseudo-inverse are represented as $(\cdot)^T$, $(\cdot)^*$, $(\cdot)^H$ and $(\cdot)^\dagger$, respectively. The operators $\text{diag}(\mathbf{q})$ and $\text{vec}(\cdot)$ represents a diagonal matrix with diagonal \mathbf{q} and the vectorized version of a matrix respectively. \mathbf{I}_Q represents a $Q \times Q$ identity matrix. Vector and Frobenius norms are denoted using $\|\cdot\|$ and $\|\cdot\|_F$ respectively.

II. SYSTEM MODEL

This work considers anchor-free localization of a UE assumed to be equipped with a uniform linear array (ULA) of length K . It is located at \mathbf{u} on the xy -plane at $z = 0$, with ULA oriented along the y axis, as shown in Fig. 1. Let r and θ be the user distance and direction with respect to the origin, respectively, such that $\mathbf{u} = r\mathbf{e}(\theta)$ and $\mathbf{e}(\theta) \triangleq [\cos \theta, \sin \theta, 0]^T$ represents the unit-vector along the direction θ . The k -th element of ULA at the UE for $k = 1, \dots, K$ is assumed to be located at $\mathbf{u}_k = \mathbf{u} + (k-1)d_u\mathbf{g}$, where d_u is the inter-antenna spacing and $\mathbf{g} = [0, 1, 0]^T$. The RIS is assumed to be located at \mathbf{s} in yz plane and have $N = N_y N_z$ elements arranged as a uniform planar array (UPA) as shown in Fig 1, where N_y and N_z represent the number of elements along y and z axes, respectively. Let d_y

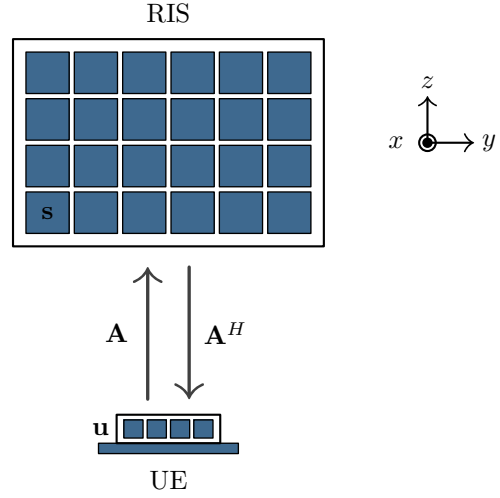


Fig. 1. RIS-assisted anchor-free localization system.

and d_z denote the RIS inter-element spacings along the y and z axes, respectively. Thus, location of the n -th element becomes $\mathbf{s}_n = \mathbf{s} + [0, (n_y - 1)d_y, (n_z - 1)d_z]^T$, such that $n \triangleq (n_y - 1)N_y + n_z$ for $n_y = 1, \dots, N_y$ and $n_z = 1, \dots, N_z$.

For the anchor-free localization, it is assumed that the UE transmits reference pulses and localizes itself using the reflected pulses from RIS. Such anchor-free localization can be performed using half duplex UE. However, it will constrain the pulse bandwidth based on the round trip delay of UE-RIS link - for instance pulse bandwidth should be > 1 MHz when the localization range is 150 meters. Alternately, similar to [14], [15], [17], a full-duplex UE can be used without enforcing the localization range limit at the cost of increased hardware complexity that is needed to cancel the self interference. Let $\mathbf{S} \in \mathbb{C}^{K \times L}$ be reference sequence matrix transmitted over L slots such that $\mathbf{S}\mathbf{S}^H = (P_T K^{-1})\mathbf{I}_K$, where P_T is the transmission power and let $\mathbf{A} \in \mathbb{C}^{N \times K}$ be the channel response of UE-RIS link. By the virtue of channel reciprocity, the channel response of RIS-UE link is conjugate-transpose of UE-RIS link. Thus, the signal received at the UE can be written as

$$\mathbf{Y} = \mathbf{A}^H \mathbf{\Omega} \mathbf{A} \mathbf{S} + \mathbf{W}, \quad (1)$$

where $\mathbf{W} \in \mathbb{C}^{K \times L}$ is zero mean complex Gaussian noise with variance σ^2 and $\mathbf{\Omega} = \text{diag}(\exp(j\boldsymbol{\omega}))$ is the diagonal RIS phase shift matrix such that $\boldsymbol{\omega} = [\omega_1, \dots, \omega_n, \dots, \omega_N]^T$ and $\omega_i \in [0, 2\pi]$. Note that the UE is assumed to be located in the near-field of RIS with dominant LoS component. Let $\mathbf{A} = [\mathbf{a}_1, \dots, \mathbf{a}_k, \dots, \mathbf{a}_K]$ such that \mathbf{a}_k is the channel between the k -th antenna element at UE and the RIS as

$$\mathbf{a}_k = \left[e^{-j2\pi\|\mathbf{u}_k - \mathbf{s}_1\|/\lambda}, \dots, e^{-j2\pi\|\mathbf{u}_k - \mathbf{s}_N\|/\lambda} \right]^T,$$

where $\|\mathbf{u}_k - \mathbf{s}_n\|$ denotes the distance between between \mathbf{u}_k and \mathbf{s}_n .

III. RIS-ASSISTED ANCHOR-FREE LOCALIZATION

This section presents the proposed RIS-assisted anchor-free localization. We first obtain an optimal configuration of RIS to improve the SNR received at UE. Next, we present a two-stage low complexity localization algorithm that utilizes the reflected signal from the optimally configured RIS.

A. Optimal RIS Configuration

Exploiting the ability of RIS to create smart propagation environment, it can be configured to improve the overall received SNR. To start with, we focus on maximizing the SNR at given UE location \mathbf{u} . For the received signal \mathbf{Y} given in (1), the SNR can be defined as

$$\text{SNR} = \frac{\|\mathbf{A}^H \boldsymbol{\Omega} \mathbf{A} \mathbf{S}\|_F^2}{\|\mathbf{W}\|_F^2} = \frac{P_T}{K} \frac{\|\mathbf{A}^H \boldsymbol{\Omega} \mathbf{A}\|_F^2}{\|\mathbf{W}\|_F^2}, \quad (2)$$

where the second equality follows from $\mathbf{S}\mathbf{S}^H = \frac{P_T}{K} \mathbf{I}_K$. Thus, the SNR maximization with respect to RIS phase matrix $\boldsymbol{\Omega}$ can be formulated as

$$\max_{\boldsymbol{\Omega}} \quad \|\mathbf{A}^H \boldsymbol{\Omega} \mathbf{A}\|_F^2, \quad (3a)$$

$$\text{s.t.} \quad \boldsymbol{\Omega} \in \mathcal{O}, \quad (3b)$$

where \mathcal{O} is a set of diagonal matrices with unit-magnitude elements. The following theorem presents the optimal phase shift matrix of RIS.

Theorem 1. *Optimal RIS phase shift matrix that maximizes the received SNR for anchor-free localization is $\boldsymbol{\Omega}_* = \mathbf{I}_N$ regardless of the location of UE.*

Proof. Using $\boldsymbol{\Omega} = \text{diag}(\exp(j\boldsymbol{\omega}))$, we vectorize $\mathbf{A}^H \boldsymbol{\Omega} \mathbf{A}$ as

$$\text{vec}(\mathbf{A}^H \boldsymbol{\Omega} \mathbf{A}) = (\mathbf{A}^T \circ \mathbf{A}^H) \exp(j\boldsymbol{\omega}),$$

where \circ denotes the Khatri-Rao product. Thus, the optimization problem in (3) can be written in vectorized form as

$$\max_{\boldsymbol{\omega}} \quad \|(\mathbf{A}^T \circ \mathbf{A}^H) \exp(j\boldsymbol{\omega})\|^2, \quad (4a)$$

$$\text{s.t.} \quad \omega_n \in [0, 2\pi] \quad \text{for } n = 1, \dots, N. \quad (4b)$$

Let $\mathbf{A} = [\boldsymbol{\alpha}_1, \dots, \boldsymbol{\alpha}_N]^T$ and let $\mathbf{H} = (\mathbf{A}^T \circ \mathbf{A}^H)$. Rewriting the Khatri-Rao product in terms of column-wise Kronecker product, we get

$$\mathbf{H} = [\boldsymbol{\alpha}_1 \otimes \boldsymbol{\alpha}_1^*, \dots, \boldsymbol{\alpha}_n \otimes \boldsymbol{\alpha}_n^*, \dots, \boldsymbol{\alpha}_N \otimes \boldsymbol{\alpha}_N^*],$$

where \otimes denotes Kronecker product. Further, we can obtain $\mathbf{C}_H = \mathbf{H}^H \mathbf{H}$ such that its (p, q) -th entry is

$$\begin{aligned} \mathbf{C}_{H,p,q} &= (\boldsymbol{\alpha}_p \otimes \boldsymbol{\alpha}_p^*)^H (\boldsymbol{\alpha}_q \otimes \boldsymbol{\alpha}_q^*) \\ &= (\boldsymbol{\alpha}_p^H \boldsymbol{\alpha}_q) \otimes (\boldsymbol{\alpha}_p^T \boldsymbol{\alpha}_q^*), \\ &= \|\boldsymbol{\alpha}_p^H \boldsymbol{\alpha}_q\|^2. \end{aligned}$$

Using this, (4a) can be simplified as

$$\begin{aligned} \|\mathbf{H} \exp(j\boldsymbol{\omega})\|^2 &= \exp(-j\boldsymbol{\omega}) \mathbf{C}_H \exp(j\boldsymbol{\omega}), \\ &= \sum_{p=1}^N \sum_{q=1}^N \exp(-j\omega_p) \mathbf{C}_{H,p,q} \exp(j\omega_q), \\ &= \sum_{p=1}^N \sum_{q=1}^N \|\boldsymbol{\alpha}_p^H \boldsymbol{\alpha}_q\|^2 \exp(j(\omega_q - \omega_p)). \end{aligned} \quad (5)$$

It can be easily seen from (5) that the received SNR can be maximized by co-phasing the terms involved in the summations. This can be achieved simply by setting $\omega_p = \omega_q$ for $\forall p, q$, i.e., all RIS elements provide the same phase shift. Thus, the optimal RIS phase shift matrix can be given as $\boldsymbol{\Omega}_* = \mathbf{I}_N$, which is independent of channel matrix \mathbf{A} . \square

Remark 1. *Since the optimal RIS phase shift matrix derived in Theorem 1 is a generalized solution that is independent of the UE location, it can be pre-configured and fixed for performing the anchor-free localization. This is a significant advantage as it does not require the exchange of any control signals between UE and RIS controller. This makes the proposed RIS-assisted anchor-free location an attractive low complex solution.*

B. Anchor-free Localization

Here, we develop a two-stage low complexity anchor-free localization algorithm. In the first stage, we obtain a coarse estimate of the UE location using the correlation of received signal with dictionary of channel matrices. In the next stage, we apply Newton refinement to obtain the optimal estimate.

1) *Coarse Estimate:* Recall from Section II that the channel matrix \mathbf{A} is uniquely characterized by the UE location parameters (r, θ) . Thus, for the optimally configured RIS with $\boldsymbol{\Omega}_* = \mathbf{I}_N$, the observed effective channel matrix can be obtained using (1) as

$$\tilde{\mathbf{Y}} = \mathbf{Y}\mathbf{S}^\dagger = \mathbf{A}^H \mathbf{A} + \tilde{\mathbf{W}}.$$

Lets consider a dictionary Φ of $\text{vec}(\mathbf{A}_m^H \mathbf{A}_m)$ defined over grid points (r_m, θ_m) for $m = 1, \dots, M$ as below

$$\Phi = \left[\begin{array}{c} \mathbf{h}_1 \\ \|\mathbf{h}_1\|, \dots, \mathbf{h}_m \\ \|\mathbf{h}_m\|, \dots, \mathbf{h}_M \\ \|\mathbf{h}_M\| \end{array} \right], \quad (6)$$

where the vector $\mathbf{h}_m = \text{vec}(\mathbf{A}_m^H \mathbf{A}_m)$ and \mathbf{A}_m is the channel from the point (r_m, θ_m) to RIS. Since \mathbf{A} represents a LoS link, the index of grid point that is nearest to UE can be identified as the column index of Φ that exhibits maximum correlation with $\tilde{\mathbf{y}} = \text{vec}(\tilde{\mathbf{Y}})$, i.e.

$$\hat{m} = \arg \max_m |\tilde{\mathbf{y}}^H \Phi_m|, \quad (7)$$

where Φ_m is the m -th column of Φ . The parameters $(r_{\hat{m}}, \theta_{\hat{m}})$ corresponding to grid point \hat{m} can be considered as the coarse estimate of UE location since the channel at \hat{m} has higher correlation with the channel observed by the UE.

2) *Newton Refinement*: The coarse estimate $(r_{\hat{m}}, \theta_{\hat{m}})$ can be refined iteratively to obtain the accurate estimate $(\hat{r}, \hat{\theta})$ of UE location. We achieve this by minimizing the error between $\tilde{\mathbf{y}}$ and $\mathbf{z} = \text{vec}(\mathbf{A}^H \mathbf{A})$ as given below

$$(\hat{r}, \hat{\theta}) = \arg \min_{r, \theta} \|\tilde{\mathbf{y}} - \mathbf{z}\|^2. \quad (8)$$

We perform Newton refinement on $(r_{\hat{m}}, \theta_{\hat{m}})$ to solve (8), as shown in Algorithm 1, with γ and τ as learning rate and tolerance respectively. The first and second order partial derivatives of $\|\tilde{\mathbf{y}} - \mathbf{z}\|^2$ are required for this, which we obtain in the following steps. The i -th element of \mathbf{z} is given by

$$z_i = \sum_{n=1}^N A_{p,q}^n, \quad (9)$$

where $i \triangleq (q-1)K + p$ and $A_{p,q}^n \triangleq a_{n,p}^* a_{n,q}$. The (n, p) -th element of \mathbf{A} is $a_{n,p} = e^{-j2\pi \|\mathbf{u}_p - \mathbf{s}_n\|/\lambda}$. Using Fresnel approximation [4], [18], we approximate $\|\mathbf{u}_p - \mathbf{s}_n\|$ as

$$\|\mathbf{u}_p - \mathbf{s}_n\| = r + \frac{(p-1)^2 d_u^2 + \|\mathbf{s}_n\|^2}{2r} + (p-1)d_u(\mathbf{e}(\theta)^T \mathbf{g} - \mathbf{g}^T \mathbf{s}_n/r) - \mathbf{e}(\theta)^T \mathbf{s}_n.$$

Using this, we rewrite $A_{p,q}^n$ as

$$A_{p,q}^n = \exp\left(\frac{-j2\pi}{\lambda} \left(\frac{d_u^2 \Delta}{2r} + d_u \delta (\mathbf{e}(\theta)^T \mathbf{g} - \mathbf{g}^T \mathbf{s}_n/r)\right)\right),$$

where $\Delta = (q-1)^2 - (p-1)^2$ and $\delta = q-p$. Let $Z_{r,n} = -j2\pi d_u (\delta \mathbf{g}^T \mathbf{s}_n - \Delta(d_u/2)) A_{p,q}^n (\lambda r^2)^{-1}$ and $Z_{\theta,n} = -j2\pi \delta d_u g_2 A_{p,q}^n \lambda^{-1}$. Using the above equation and (9), the derivatives of z_i with respect to r and θ can be determined as

$$\begin{aligned} \frac{\partial z_i}{\partial r} &= \sum_{n=1}^N Z_{r,n}, \\ \frac{\partial^2 z_i}{\partial r^2} &= \sum_{n=1}^N Z_{r,n} (Z_{r,n} - 2r^{-1}), \\ \frac{\partial z_i}{\partial \theta} &= \sum_{n=1}^N Z_{\theta,n} \cos \theta \text{ and} \\ \frac{\partial^2 z_i}{\partial \theta^2} &= \sum_{n=1}^N Z_{\theta,n} (Z_{\theta,n} \cos^2 \theta \lambda^{-1} + \sin \theta). \end{aligned}$$

Let $\frac{\partial \mathbf{z}}{\partial \kappa} = [\frac{\partial z_1}{\partial \kappa}, \dots, \frac{\partial z_{K^2}}{\partial \kappa}]^T$ and $\frac{\partial^2 \mathbf{z}}{\partial \kappa^2} = [\frac{\partial^2 z_1}{\partial \kappa^2}, \dots, \frac{\partial^2 z_{K^2}}{\partial \kappa^2}]^T$ for $\kappa \in \{r, \theta\}$. Thus, the first-order and second-order partial derivatives of $\beta = \|\tilde{\mathbf{y}} - \mathbf{z}\|^2$ with respect to r and θ are

$$\frac{\partial \beta}{\partial r} = -2 \text{Re} \left\{ (\tilde{\mathbf{y}} - \mathbf{z})^H \frac{\partial \mathbf{z}}{\partial r} \right\}, \quad (10)$$

$$\frac{\partial^2 \beta}{\partial r^2} = 2 \left\| \frac{\partial^2 \mathbf{z}}{\partial r^2} \right\|^2 - 2 \text{Re} \left\{ (\tilde{\mathbf{y}} - \mathbf{z})^H \frac{\partial^2 \mathbf{z}}{\partial r^2} \right\}, \quad (11)$$

$$\frac{\partial \beta}{\partial \theta} = -2 \text{Re} \left\{ (\tilde{\mathbf{y}} - \mathbf{z})^H \frac{\partial \mathbf{z}}{\partial \theta} \right\} \text{ and} \quad (12)$$

$$\frac{\partial^2 \beta}{\partial \theta^2} = 2 \left\| \frac{\partial^2 \mathbf{z}}{\partial \theta^2} \right\|^2 - 2 \text{Re} \left\{ (\tilde{\mathbf{y}} - \mathbf{z})^H \frac{\partial^2 \mathbf{z}}{\partial \theta^2} \right\}, \quad (13)$$

where $\text{Re}(\cdot)$ denotes the real part of a complex number. Thus, these partial derivatives can be employed to iteratively refine the coarse estimate $(r_{\hat{m}}, \theta_{\hat{m}})$ as described in Algorithm 1.

Algorithm 1: RIS-assisted Anchor-free Localization

Inputs: $\tilde{\mathbf{y}}, \Phi, \gamma$ and τ

Outputs: $\hat{r}, \hat{\theta}$

- 1 Evaluate $\hat{m} = \arg \max_m |\tilde{\mathbf{y}}^H \Phi|$
 - 2 Find $r_{\hat{m}}$ and $\theta_{\hat{m}}$ corresponding to \hat{m}
 - 3 Set $i = 0, r_0 = r_{\hat{m}}$ and $\theta_0 = \theta_{\hat{m}}$
 - 4 **Repeat**
 - 5 Evaluate $\delta_{r,i}$ and $\delta_{\theta,i}$ using (10) to (13) as

$$\delta_{r,i} = \frac{\partial \beta}{\partial r_i} \left(\frac{\partial^2 \beta}{\partial r_i^2} \right)^{-1}$$

$$\delta_{\theta,i} = \frac{\partial \beta}{\partial \theta_i} \left(\frac{\partial^2 \beta}{\partial \theta_i^2} \right)^{-1}$$
 - 6 Update

$$r_{i+1} = r_i - \gamma \delta_{r,i}$$

$$\theta_{i+1} = \theta_i - \gamma \delta_{\theta,i}$$

$$i = i + 1$$
 - 7 **Until** $|r_i - r_{i-1}| < \tau$ and $|\theta_i - \theta_{i-1}| < \tau$;
 - 8 Set $\hat{r} = r_i$ and $\hat{\theta} = \theta_i$
-

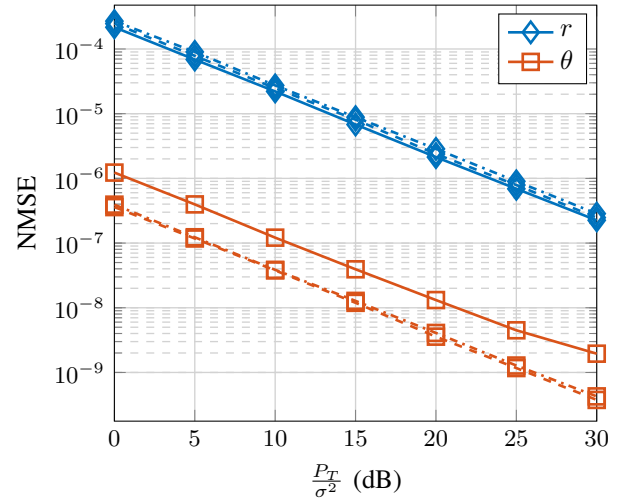


Fig. 2. NMSE of UE location (r, θ) for $K = 8$. The solid, dashed and dot-dashed lines correspond to $N = 64, N = 121$ and $N = 256$ respectively.

IV. NUMERICAL RESULTS AND DISCUSSION

This section presents the numerical analysis of the NMSE performance of Algorithm 1. For the numerical results, we considered the parameters as number of RIS elements N with $N_y = N_z = \sqrt{N} \in \{8, 10, 11, 12\}$, operational wavelength $\lambda = 0.1$ m, transmission power $P_T = 30$ dBm, number of transmission slots L equal to number of UE antenna K , learning rate $\gamma = 0.5$ and tolerance $\tau = 10^{-4}$; unless mentioned otherwise. We define the near-field region between Fresnel distance $0.62\lambda^{-1/2} (a_R^2 + b_R^2)^{3/4}$ and Rayleigh distance $2\lambda^{-1} (a_R^2 + b_R^2)$ [4], [18], where $a_R = (N_y - 1)d_y$ and $b_R = (N_z - 1)d_z$ denote the dimensions of the RIS along y and z axes. To construct the dictionary Φ , we sample the

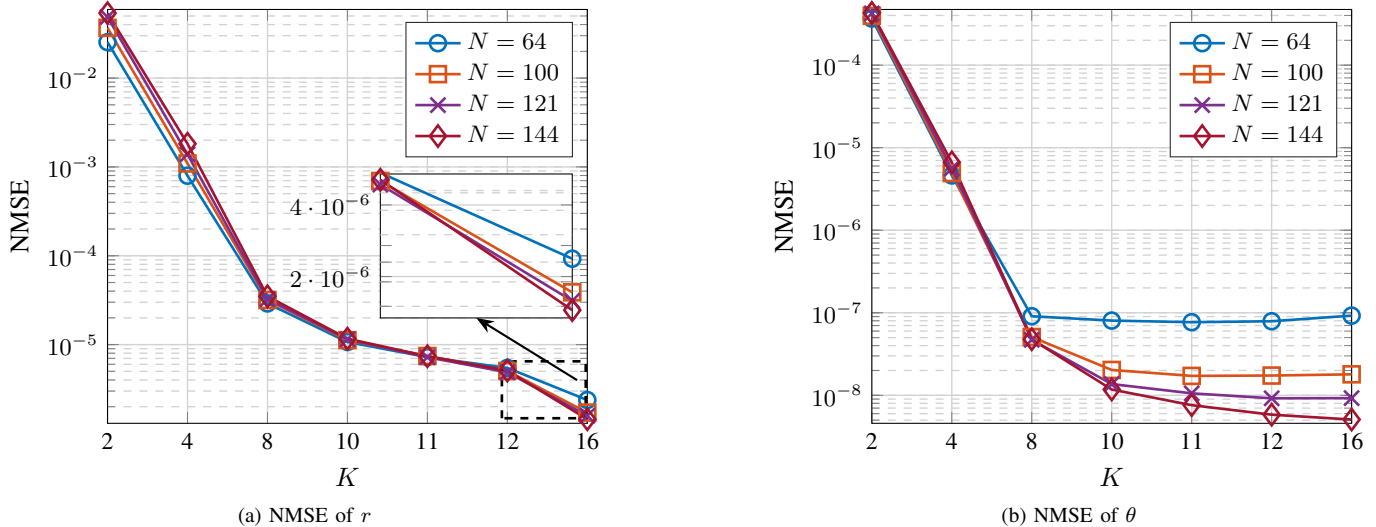


Fig. 3. NMSEs of r and θ for $P_T/\sigma^2 = 10\text{dB}$.

grid points in the near-field with a resolution of $\epsilon = 0.55\text{m}$ along x and y axes. We perform the Monte Carlo simulation with 10,000 iterations to evaluate the NMSE performance of the proposed algorithm. In each iteration, we sample the UE location (r, θ) uniformly at random in the near-field region.

Fig. 2 shows that the NMSE performance improves with the increase in SNR, as expected. It can be also observed that the NMSE of r slightly degrades as the number of RIS elements N increases. This may be attributed to the fact that the larger RISs extend the span of near-field, leading to some loss of performance which is almost compensated by the higher array gain achieved with the increased RIS size. This makes the proposed algorithm scalable to large RIS scenario without degrading the NMSE of r . Besides, the improvement in NMSE of θ with increase in N saturates at moderately higher values of N .

The effective channel gain with optimally configured RIS is $\|\mathbf{A}^H \mathbf{A}\|_F^2$ which increases quadratically with number of antennas at UE K and number of RIS elements N . Thus, it is natural that the NMSE of both r and θ improves with the increase in either N or K or both, as can be verified from Fig. 3. However, Fig. 3a shows some degradation in performance of r with increase in N for small values of K . This is because, as highlighted earlier, increase in N results in larger span of r . Interestingly, the overall increase in channel gain obtained at higher values of K and N over compensates for the degradation caused due to increased span at higher N , which in turn gives better NMSE for r . Fig. 3b shows the similar NMSEs of θ for all N until the saturation occurs at corresponding values of $K = \sqrt{N}$. In other words, the improvements in NMSE of θ with increase in N occur at larger values of K . This is because the larger N allows the NMSE to drop till a corresponding larger K and thus the relative performance improvement with respect to N is visible at larger K .

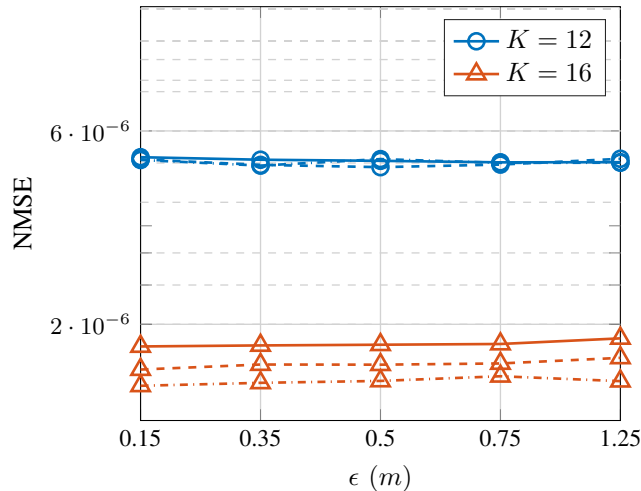
To assess the performance of the Newton refinement, Fig. 4 presents the impact of grid resolution ϵ on the NMSE performance of UE location and the number of iterations required for the convergence of Algorithm 1. Fig. 4a shows that the NMSE performance is similar regardless of the resolution ϵ , which ensures the robust refinement of the coarse estimate obtained with a smaller dictionary. However, Fig. 4b shows that the number of iterations needed to refine the coarse estimate increases with the increase in ϵ , as is expected. The rate of increase in the number of iterations becomes insignificant at larger K regardless of N . However, the number of iterations required are larger for smaller K .

V. CONCLUSION

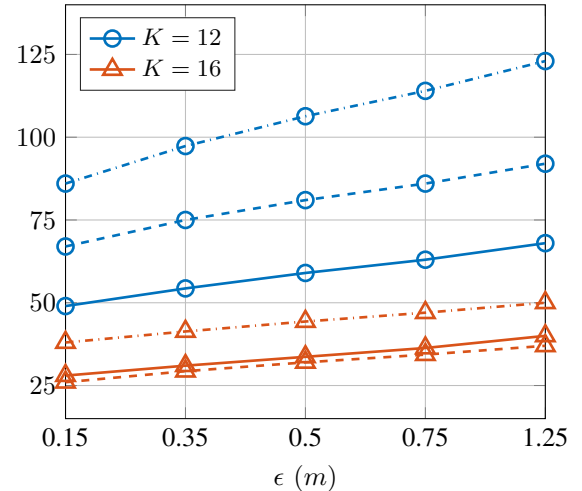
In this work, we proved that the optimal RIS phase shift matrix that maximizes the received SNR can be pre-configured using a generalized solution that is independent of UE location. Further, we presented a two-stage anchor-free localization algorithm that 1) utilizes a dictionary of near-field channels to enable coarse estimation and 2) employs Newton refinement on these estimates to iteratively refine it. Through extensive numerical analysis, we demonstrated the NMSE performance remains mostly unaffected by enlarging the the near-field localization region via increasing the number of RIS elements, which ensures that the proposed approach is scalable to practical settings. In addition, the proposed algorithm provides robust performance even with a small-sized dictionary (constructed using fewer reference points) based coarse estimation.

REFERENCES

- [1] K. Keykhosravi and et.al., "Leveraging RIS-enabled smart signal propagation for solving infeasible localization problems: Scenarios, key research directions, and open challenges," *IEEE Vehicular Technology Magazine*, vol. 18, no. 2, pp. 20–28, 2023.



(a) NMSE performance of UE location u .



(b) Number of iteration

Fig. 4. Impact of grid resolution ϵ on NMSE performance and number of iterations for $P_T/\sigma^2 = 10\text{dB}$. The solid, dashed and dot-dashed lines correspond to $N = 100$, $N = 121$ and $N = 144$ respectively.

- [2] Y. Zhao and et al., “6G near-field technologies white paper 2.0,” 2025. [Online]. Available: <https://eprints.gla.ac.uk/354426/>
- [3] A. Bourdoux and et. al., “6G white paper on localization and sensing,” 2020. [Online]. Available: <https://arxiv.org/abs/2006.01779>
- [4] S. S. Sadhu, P. D. Mankar, and S. Nannuru, “Near-field 5D pose estimation using reconfigurable intelligent surfaces,” in *IEEE Global Communications Conference (GLOBECOM)*, 2025. [Online]. Available: <https://arxiv.org/abs/2505.01829>
- [5] S. Basharat, S. A. Hassan, H. Pervaiz, A. Mahmood, Z. Ding, and M. Gidlund, “Reconfigurable intelligent surfaces: Potentials, applications, and challenges for 6G wireless networks,” *IEEE Wireless Communications*, vol. 28, no. 6, pp. 184–191, 2021.
- [6] J. A. del Peral-Rosado, R. Raulefs, J. A. López-Salcedo, and G. Seco-Granados, “Survey of cellular mobile radio localization methods: From 1G to 5G,” *IEEE Communications Surveys & Tutorials*, vol. 20, no. 2, pp. 1124–1148, 2018.
- [7] L. Cheng, C. Wu, Y. Zhang, H. Wu, M. Li, and C. Maple, “A survey of localization in wireless sensor network,” *International Journal of Distributed Sensor Networks*, vol. 8, no. 12, p. 962523, 2012.
- [8] F. Zafari, A. Gkelias, and K. K. Leung, “A survey of indoor localization systems and technologies,” *IEEE Communications Surveys & Tutorials*, vol. 21, no. 3, pp. 2568–2599, 2019.
- [9] T. K. Mishra and et al., “An enhanced path planning model for anchor-free localization in wireless sensor networks,” in *International Conference on Information Technology (ICIT)*, 2018, pp. 204–209.
- [10] V. C. S. R. Rayavarapu and A. Mahapatro, “A novel range-free anchor-free localization in WSN using sun flower optimization algorithm,” in *2021 Advanced Communication Technologies and Signal Processing (ACTS)*, 2021, pp. 1–6.
- [11] H. A. G. C. Premachandra and et al., “UWB radar SLAM: An anchorless approach in vision denied indoor environments,” *IEEE Robotics and Automation Letters*, vol. 8, no. 9, pp. 5299–5306, 2023.
- [12] X. Cai, L. Wang, S. Sun, H. Han, and K. Han, “Anchor-free relative 3D pose estimation using ultra-wideband and inertial data fusion,” in *2024 IEEE SENSORS*, 2024, pp. 1–4.
- [13] H. Chen, H. Kim, M. Ammous, G. Seco-Granados, G. C. Alexandropoulos, S. Valaee, and H. Wymeersch, “RISs and sidelink communications in smart cities: The key to seamless localization and sensing,” *IEEE Communications Magazine*, vol. 61, no. 8, pp. 140–146, 2023.
- [14] K. Keykhosravi, G. Seco-Granados, G. C. Alexandropoulos, and H. Wymeersch, “RIS-enabled self-localization: Leveraging controllable reflections with zero access points,” in *ICC 2022 - IEEE International Conference on Communications*, 2022, pp. 2852–2857.
- [15] H. Kim, H. Chen, M. F. Keskin, Y. Ge, K. Keykhosravi, G. C. Alexandropoulos, S. Kim, and H. Wymeersch, “RIS-enabled and access-point-free simultaneous radio localization and mapping,” *IEEE Transactions on Wireless Communications*, vol. 23, no. 4, pp. 3344–3360, 2024.
- [16] M. Ammous, H. Chen, H. Wymeersch, and S. Valaee, “3D cooperative positioning via RIS and sidelink communications with zero access points,” *IEEE Transactions on Mobile Computing*, vol. 24, no. 7, pp. 6119–6136, 2025.
- [17] N. Hyowon Kim, M. F. Keskin, Z. S. He, J. Gil, G.-S. Granados, and H. Wymeersch, “RIS-enabled self-localization with FMCW radar,” 2025. [Online]. Available: <https://arxiv.org/abs/2503.21021>
- [18] Y. Liu, Z. Wang, J. Xu, C. Ouyang, X. Mu, and R. Schober, “Near-field communications: A tutorial review,” *IEEE Open Journal of the Communications Society*, vol. 4, pp. 1999–2049, 2023.